Bulletin of the Seismological Society of America, Vol. 86, No. 6, pp. 1770–1783, December 1996

A Neotectonic Study of the San Miguel–Vallecitos Fault, Baja California, Mexico

by C. Kenji Hirabayashi, Thomas K. Rockwell, Steven G. Wesnousky, Mark W. Stirling, and Francisco Suarez-Vidal

Abstract The San Miguel strand of the San Miguel–Vallecitos fault zone displaces an alluvial ridge $23^{+5}/_{-10}$ m in the vicinity of Dolores Mountain. The same section of fault produced surface rupture during the *M*6.8 earthquake of 1956. We estimate a minimum age of the ridge at between $110^{+150}/_{-60}$ ka by comparing soil development on the offset ridge to two soil chronosequences in southern California. Dividing the measured offset by the age of the ridge places a maximum range on the fault slip rate of $0.2^{+0.35}/_{-0.15}$ mm/yr. Excavations along and across the fault at the same site revealed at least 80 cm and probably 115 cm of right-lateral offset of a now-buried stream channel deposit. We attribute the 115-cm offset to the 1956 *M*6.8 earthquake, a displacement that is slightly larger than previously reported for this earthquake. Dividing the 80 to 115 cm of displacement by the calculated fault slip rate yields an estimated return time for similar-sized events of about $5.8^{+17}/_{-4.3}$ ka. Similarly, dividing the slip expected for rupture of the entire 160-km length of the San Miguel–Vallecitos fault zone by the fault slip rate yields an estimate of return time of M_w7.8 earthquakes of about 80 ka. The slip rate determined from this study is at least an order of magnitude less than that contributed by the Agua Blanca fault and indicates that the San Miguel fault zone transfers less than about 1% of the plate motions.

The San Miguel fault shows a complex fault trace and registers a small value of cumulative geologic offset (maximum of 0.6 km). When combining the geological estimates of magnitude and return time of the largest earthquakes with magnitude–frequency data recorded along the San Miguel fault by the RESNOR seismic network during the period 1976 to 1991, we observe that the shape of the magnitude–frequency distribution along the fault may be described by the Gutenberg–Richter relationship $\text{Log } n = a - bM$. In contrast, along-strike-slip faults in southern California that are characterized by orders of magnitude more cumulative offset and less complex fault traces, we observe that extrapolation of earthquake frequency statistics from the instrumental record of seismicity severely underestimates the rate of occurrence of maximum expected events. We speculate that the relatively high productivity of small earthquakes along the San Miguel fault reflects a more heterogeneous stress field associated with the incipient and complex nature of the fault trace.

Introduction

The San Miguel–Vallecitos fault zone strikes southeastward for a distance of about 160 km from the vicinity of Tijuana (Shor and Roberts, 1958) (Fig. 1). The fault zone, located within the peninsular ranges of Baja California, is one of many faults in southern California and Baja California that has produced moderate to large earthquakes in historic time, and it accommodates relative motion between the Pacific and North American plates. The fault zone is composed of the Vallecitos, Calabasas, and San Miguel fault strands (Shor and Roberts, 1958; Gastil *et al.,* 1975) (Fig. 1). The fault zone displays right-lateral strike-slip motion (e.g., Doser, 1992; Shor and Roberts, 1958) and appears to be the southeastward extension of the Rose Canyon fault zone that cuts the metropolitan San Diego region and, in turn, strikes northward along the California coast. However, there are some structural complexities that separate the Rose Canyon and San Miguel fault zones.

The San Miguel fault zone has been the most seismi-

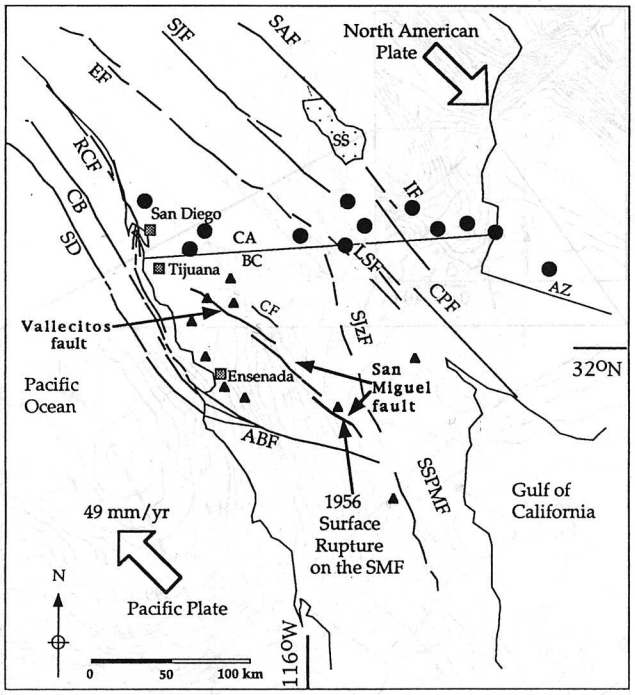

Figure 1. Regional map showing the relation of the San Miguel fault to other major faults in southern California and northern Baja California. RESNOR seismic network sites are denoted by solid triangles, and the southernmost CIT–USGA stations are denoted by circles. SAF, San Andreas fault; SJF, San Jacinto fault; EF, Elsinore fault; RCF, Rose Canyon fault; IF, Imperial fault; CPF, Cerro Prieto fault; LSF, Laguna Salada fault; SJzF, Sierra Juarez fault; ABF, Agua Blanca fault; CF, Calabasas fault; SSPMF, Sierra San Pedro Martir fault; SMF, San Miguel fault; SS, Salton Sea; CB, Coronado Bank fault; SD, San Diego Trough fault; Ca, California; AZ, Arizona; BC, Baja California.

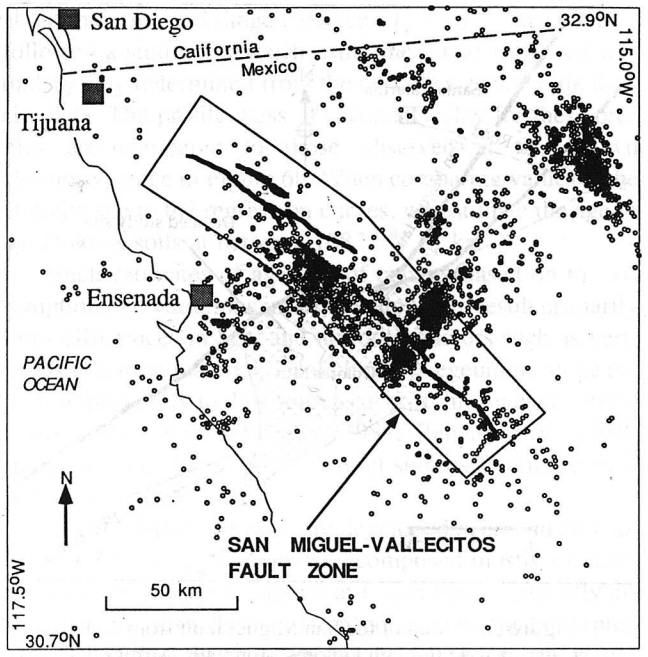

Figure 2. Epicentral map of all earthquakes in northern Baja California, Mexico, recorded by RESNOR (1976 to 1991). Analysis of seismicity to construct Figure 14a is limited to area within polygon.

cally active structure of the Baja California peninsula this century (Reyes *et al.,* 1975), producing six moderate earthquakes of about magnitude 6 or greater in a sequence from 1954 to 1956 on the San Miguel fault segment alone. Microearthquake records display abundant seismic activity along the fault zone, particularly on the San Miguel fault (Fig. 2) (Reyes *et al.,* 1975; Johnson *et al.,* 1976; Vidal and Munguia, 1991). Previous work by Harvey (1985) and Giroux (1993) determined total offset on the fault zone to be no greater than 0.5 to 0.6 km based on reconstructed Mesozoic features.

In this article, we combine seismological observations with a fault slip rate and paleoearthquake study of the fault to place further limits on the slip budget of southern California borderland faults and, hence, the seismic hazard in San Diego and the greater southern California region. Furthermore, we examine the relationship between seismicity, cumulative geologic offset, and the structural complexity of strike-slip faults to better understand the relationships between the evolution of faults and their seismic productivity, as well as their potential to generate large earthquakes.

Geological Observations

Four earthquakes of magnitude between 6 and 6.8 occurred along the southern portion of the San Miguel–Vallecitos fault zone between 9 and 15 February 1956. Shor and Roberts (1958) conducted field investigations shortly after the sequence and documented 20 km of surface rupture extending along the southern end of the zone. They labeled this surface rupture as the San Miguel fault (Fig. 1). The sense of motion was determined to be right-oblique, with horizontal and vertical motions reaching to about 0.8 and 0.9 m, respectively, and vertical motion generally being up to the east. More recently, Doser (1992) determined mostly dextral strike-slip focal mechanisms for the 1956 mainshock and principal aftershocks, in contrast to some of the field observations.

Harvey (1985) reexamined the trace in the field using 1:50,000 scale airphotos taken by the U.S. military in 1956 shortly after the earthquake sequence. He found that the 1956 rupture trace was still relatively well preserved only along a 4-km section of the fault near Dolores Mountain (Fig. 3). We returned in 1992 and 1993 to the section of fault east of Santa Catarina road (Fig. 3) in the vicinity of Dolores Mountain and conducted both a fault slip rate and paleoearthquake study (Hirabayashi, 1995).

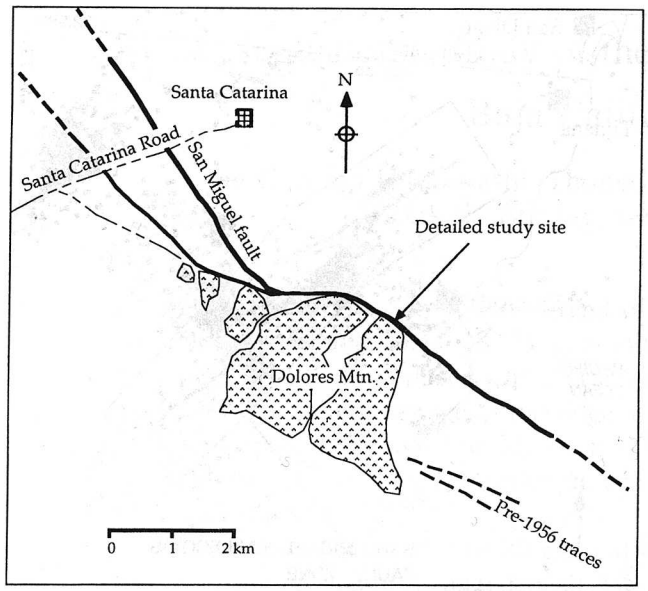

Figure 3. Map of the San Miguel fault from Santa Catarina road through Dolores Mountain. Arrows denote the 1956 rupture. Note that in the area of our trenching, there is only one primary rupture trace, as opposed to two traces to the northwest. Also note the southern trace that did not rupture in 1956. The patterned areas at and around Dolores Mountain indicate Miocene volcanic rocks at the surface; all other exposed rocks are granitic.

Late Quaternary Slip Rate of the San Miguel Fault

The San Miguel fault crosses a linear ridge within a small drainage valley on the northeast side of Dolores Mountain. Composed of Tertiary alluvial deposits of Rodeo Gravel (Minch, 1979) and partially capped by alluvial fan deposits, the ridge is bound by channels that are incised into these deposits, preserving a relatively straight, flat-crested ridgeline that was subsequently offset by the fault (Figs. 4 and 5). Two splays offset the ridge in a right-lateral sense, with the northeast strand shown as a prominent, southwest-facing scarp; this strand is responsible for the majority of ridge offset. Offset is expressed across the southwest strand, which is marked by a small linear depression. The topographic map of the ridge shown in Figure 4 was constructed by surveying over 450 points with a Wild TC2000 total station (Fig. 4). Reconstruction of the offset ridge crest places a dextral displacement at $23^{+5}/_{-10}$ m, where the error reflects the uncertainty in defining the centerline of the ridge crest (Fig. 5). In this reconstruction, we observe that the ridgeline is relatively straight north and south of the fault zone, so we assume that the measured deflection represents slip. Another estimate of the lateral slip can also be made by measuring the offset of the margins of the flat-crested portion of the ridge, in which case estimates of offset range between 13 and 28 m. The smaller estimate is made from reconstruction of the northwest margin, which has been modified by erosion as the ridgeline is shunted northwest-

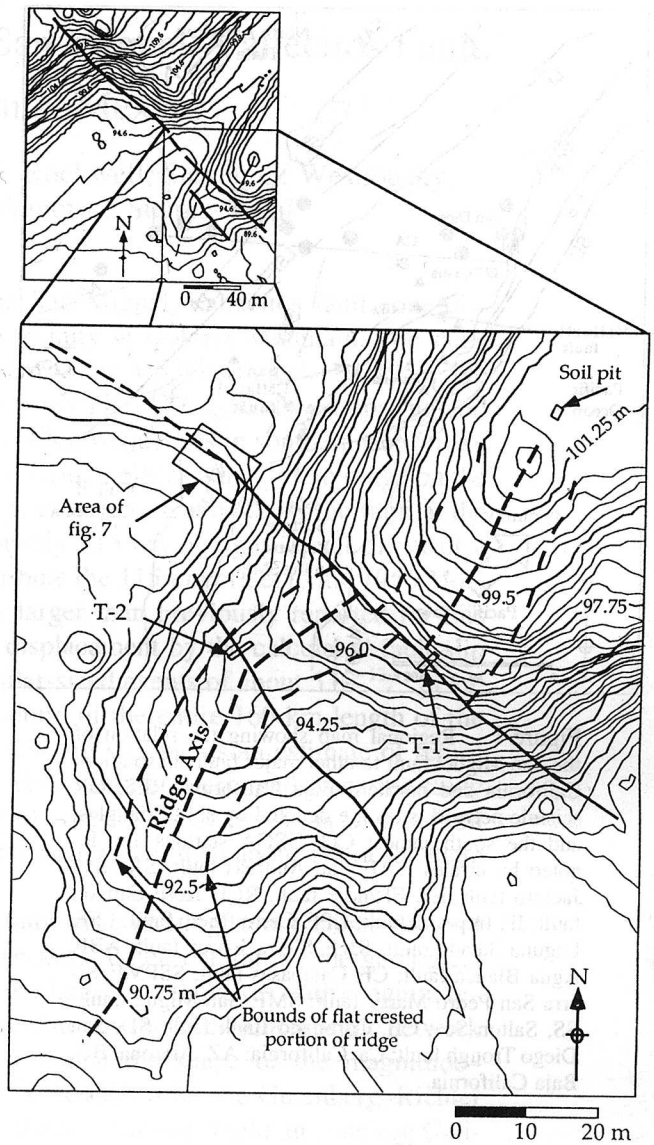

Figure 4. Map showing portion of fault trace on the east side of Dolores Mountain and enlargement of an offset alluvial ridge. Note the locations of the soil pit and trenches T-1 and T-2. The area of 3D investigation is shown as the area of Figure 7. Dashed lines represent the ridge axis, dotted lines represent the margins of the flat-crested portion of the ridge, and bold lines represent fault strands. Contour interval is 0.35 m.

ward into the active drainage. Consequently, the 13-m estimate is probably a minimum.

To estimate the age of the offset ridge, we collected two soil profiles (SP1A and SP1B) in the soil pit at the crest of the ridge within the capping alluvial unit and two soil profiles (T2A and T2B) developed in Rodeo Gravel exposed in trench T-2 (Fig. 4). The alluvium capping the ridge sits upon Tertiary Rodeo Gravel to the northeast of the main fault strand. Southwest of the fault, trench T-2 shows that the

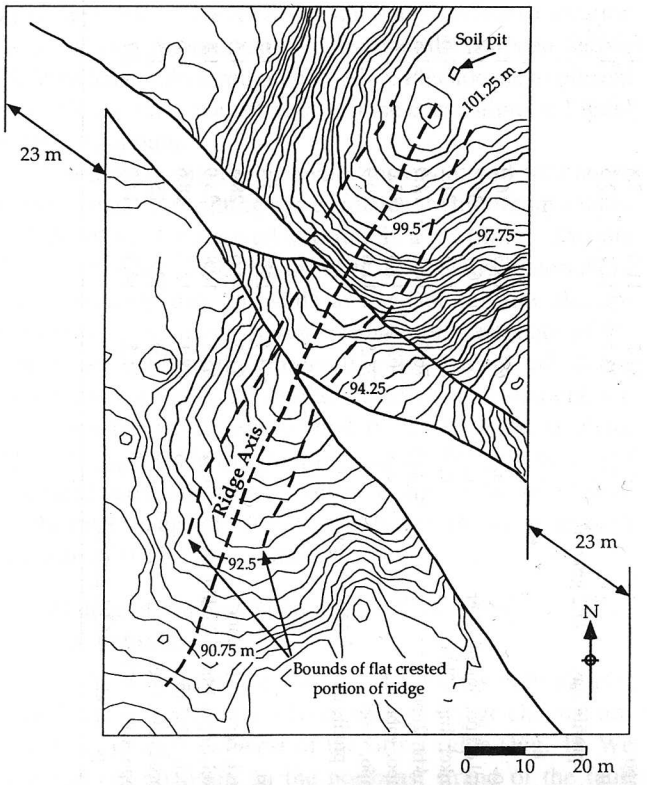

Figure 5. Reconstruction of the centerline of the offset alluvial ridge, shown in Figure 4, used to determine the best estimate of lateral displacement. Dashed lines represent the ridge axis and the margins of the flat-crested portion of the ridge, and bold lines represent fault strands.

ridge is composed of Rodeo Gravel without the alluvial cap. Each of the profiles is described and analyzed according to standard techniques (Soil Survey Staff, 1975) and summarized in Table 1. The soil profiles were quantified by determining both the soil development index (SDI) of Harden (1982) and the mass accumulation of profile clay with bulk density and particle size analysis (Table 1). Although we were unable to place any direct radiometric age constraints on the ages of soil development, we place bounds on the ages of the soil profiles by comparing the SDI values and the mass accumulation of profile clay to those observed in dated chronosequences in southern California, developed under similar environmental conditions.

We compared the SDI values determined for the Dolores Mountain profiles to those reported for dated chronosequences at Merced (Harden, 1982) and Cajon Pass (McFadden and Weldon, 1987) (Fig. 6). Profiles at each of the sites were normalized to 2.5 m (Birkeland, 1984). A linear least-squares fit and 95% confidence limits using t statistics are drawn in Figure 6a for the values of age and SDI for the known chronosequences. It may be inferred by placing the SDI values determined for the Dolores profiles onto the regression lines that the Dolores profile ages are all about the same and range between $113^{+122}/_{-46}$ ka. We also followed a similar approach using measured values of secondary clay determined from the particle size and bulk density data. The profile mass of secondary clay for these profiles are compared to those observed at the known chronosequence in Figure 6b. When comparing values at the Dolores site to the regression curves, we estimate the age of the Dolores soils at between $108^{+144}/_{-56}$ ka.

Such estimates of age are, of course, based on the assumption that variations in soil development result primarily from differences in age, and not other factors such as variations in parent material, local climate, vegetation, slope aspect, or proximity to dust sources (e.g., Johnson *et al.,* 1990; Johnson and Watson-Stegner, 1987; Reheis *et al.,* 1989; Harrison *et al.,* 1990, 1993). A brief summary of these variables is provided below.

Dolores Mountain soils are developed in eroded alluvial fan and Tertiary gravel deposits composed mostly of gravelly sand. Soil parent material at Cajon Pass is gravelly alluvium with clasts derived from granitic and metamorphic sources (McFadden and Weldon, 1987; Rockwell *et al.,* 1990), whereas Merced soils are developed in nongravelly granitic alluvium (Harden, 1982). The clasts in the Dolores Mountain deposits are derived mainly from granitic, volcanic and metamorphic sources. Once erosion occurred and the surface stabilized, the ridge material derived from the Tertiary deposits should behave more or less as alluvium in the development of soils. Nevertheless, the erosional nature of these deposits indicates that the resulting soil-age estimates should be considered minimum values for the actual age of the ridgeline.

Present annual rainfall amounts for Cajon Pass (63 to 73 cm) and Merced (41 cm) are higher than Dolores Mountain (17 to 22 cm from 1958 to 1964). Dolores Mountain (1900 m, 15 to 16 °C) is significantly higher in elevation but of similar annual temperature when compared to the Cajon Pass (710 to 950 m, 16.5 °C) and Merced (20 to 200 m, 16 °C) study sites. The largest apparent discrepancy between Dolores Mountain and the other study sites is the difference in precipitation due to the latitude and elevation of the study site. Lower rainfall, producing lower illuviation rates, would slow the soil development, yielding too young an apparent age for the soil. However, the six years of recorded rainfall for Dolores Mountain may not be representative of the longer-term average, and if it is, most of the soil development occurred principally during the Pleistocene when rainfall differences between the sites cannot be accurately estimated. The character of the Dolores Mountain soil is more akin to an Alfisol with a thinned A horizon and a rubified and relatively thick B_t horizon, supporting higher levels of annual rainfall than recorded in those 6 years. Furthermore, there is no calcic horizon as expected with an arid climate, suggesting that either precipitation was high enough during the late Pleistocene to leach the soil of soluble salts and carbonate, and there has been no significant recharge of salts during the Holocene, or that the actual Holocene rain-

Table 1

Soil Profiles of the Dolores Mountain–San Miguel Fault

Horizon	Depth, cm	T, cm	Color	Texture	Structure	Consistency		Clay Films	Boundary	Sand %	Silt %	Clay %	Bulk Density
						Dry	Wet						
Profile SP1A													
A	0–8	8.0	7.5YR 5/3d; 4/2m	SL	2f-mcr	sh	s, ps	n.o.	a, s	66.0	17.1	17.0	1.3
Bt1	8–25	17.0	5YR 6/4d; 5/6m	SCL	2.5mabk	vh	2, p	3mkcl, 2mkpo, 2copf, 3kbr	c, w	64.8	14.2	21.0	1.7
Bt2	25–45	20.0	5YR 6/6d; 5/6m	SCL	2.5mabk	vh-eh	vs, vp	3mkcl, 1npo, 1npf, 1mkbr	1, w	67.5	12.0	20.5	1.7
BC1	45–84	39.0	7.5YR 7/4d; 6/6m	SL	lf-msbk	vh	s, vp	1ncl, 1nbr	c, w	70.8	12.4	16.9	1.8
BC2	84–135	51.0	7.5YR 8/4d; 7/4m	SL	1fsbk	vh-eh	ss, ps	vnbr, vmkcl	a, w	78.9	12.0	9.1	1.8
2BC1	135–167	32.0	10YR 7/3d; 6/4m	LS	1fsbk	h	so, po	vnbr	a, w	83.4	10.1	6.5	1.7
3BC	167–199+	32.0	10YR 7/4; 6/4m	LS	1fsbk	sh	so, po	n.o.		79.7	11.9	8.4	1.6
			SDI = 81.2					profile clay = 47.8 gm/cm2					
Profile SP1B													
A	0–2	2.0	7.5YR 4/3d; 3/2m	SL	2fcr	s	s, p	n.o.	a, w	69.8	15.7	14.5	1.5
Bt1	2–20	18.0	5YR 5/6d; 4/6m	SL	2.5msbk	sh	s, p	3mkcl, 1npo, 1copf, 3mkbr	a, w	69.2	13.5	17.3	1.6
Bt2	20–39	19.0	5YR 6/6d; 5/6m	SCL	3cabk	eh	vs, vp	2mkcl, 1npo, 3kbr	a, s	68.2	11.6	20.3	1.7
BC1	39–77	38.0	7.5YR 7/4d; 6/6m	SL	1fsbk	h	s, ps	2ncl, 2mkbr	c, w	71.5	13.0	15.5	1.7
BC2	77–148	71.0	7.5YR 8/4d; 7/3m	SL	1fsbk	sh	s, ps	vnbr	a, w	77.8	11.8	10.4	1.8
2BC1	148–184	36.0	10YR 7/4d; 6/4m	LS	1fsbk	h	ss, po	1npo	c, w	81.2	11.0	7.8	1.7
3Cox	184–196+	12.0	10YR 7/4d; 6/4m	SL	1sbk	sh-h	ss, ps	n.o.		73.1	14.4	12.5	1.5
			SDI = 79.6					profile clay = 47.2 gm/cm2					
Profile T2A													
A	0–10	10.0	7.5YR 5/4d; 4/2m	SL	1msbk	h	s, p	n.o.	a, s	65.7	18.3	16.0	1.4
Bt1	10–24	14.0	5YR 5/4d; 4/4m	SCL	3fabk	vh-eh	s, ps	3kcl, 2kpo, 3mkpf, 2kbr	c, s	51.8	16.5	31.8	1.5
Bt2	24–49	25.0	7.5YR 6/4d; 5.4m	SCL	2fsbk	vh-eh	s, p	3mkcl, 1npo, 2kbr	c, w	67.5	11.3	21.2	1.6
BC1	49–87	38.0	7.5YR 6/6d; 5/6m	SL	1f-msbk	sh	ss, ps	1mkbr, 2npo	g, w	76.0	10.1	14.0	1.8
BC2	87–123	36.0	7.5YR 7/4d; 6/4m	SL	1fsbk	sh	ss, ps	vnpo, vnbr	c, s	76.2	11.8	12.0	1.6
BC3	123–193+	70.0	10YR 7/4d; 5/4m	SL	1fsbk	h	ss, ps	vnpo, vcocl		77.5	11.6	10.9	1.7
			SDI = 83.4					profile clay = 57.8 cm/gm2					
Profile T2B													
A	0–7	7.0	10YR 5/3d; 3/2m	SL	2mcr	s	s, p	n.o.	a, s	69.4	15.3	15.3	1.2
Bt1	7–24	17.0	5YR 4/6d; 4/6m	SCL	2f-msbk	sh	vs, vp	3kcl, 2npo, 1npf, 2nbr	a, s	57.5	14.0	28.5	1.6
Bt2	24–48	24.0	7.5YR 4/4d; 4.6m	SCL	3f-msbk	vh-eh	vs, vp	2kcl, 2npo, 1mkpf, 2mkbr	c, s	65.3	10.8	23.9	1.5
BC1	48–69	21.0	7.5YR 6/6d; 5/6m	SL	1msbk	h	s, p	1ncl, 1nbr, 1npo	c, s	68.1	13.3	18.6	1.6
BC2	69–109	40.0	7.5YR 8/3d; 6/4m	SL	2fsbk	h	ss, p	2npo, vnbr, vncl	c, s	72.9	12.0	15.1	1.5
BC3	109–193+	84.0	7.5YR 7/4d; 5/6m	SL	1fsbk	sh	ss, sp	2npo, vnbr, vncl		71.5	14.3	14.2	1.7
			SDI = 93.9					profile clay = 63.1 gm/cm2					

fall is higher here due to the substantially increased elevation of the region. In summary, if the rainfall has been less at Dolores Mountain throughout the late Pleistocene to present time, the ages that we determine in the correlations in Figure 6 are a minimum.

Therefore, considering major factors of soil formation, we infer that the resulting age estimates are minimum values, and therefore, the derived slip rate is a maximum. Despite the uncertainties, and the inability to provide materials to radiometrically date the soils at the Dolores site, the approach we have used provides a first-order estimate of the time taken to form the observed soils. Because all of the soil profiles are at very similar stages of development, we infer that the entire surface and ridge stabilized at about $110^{+150}/_{-60}$ ka. Hence, dividing the $23^{+5}/_{-10}$ m best estimate and maximum range of inferred slip for the offset ridge by the inferred age of the ridge yields an estimate of the fault slip rate of $0.2^{+0.35}/_{-0.15}$ mm/yr.

Timing of Surface Ruptures and Coseismic Slip Estimates

We also excavated a number of trenches both parallel to and across the fault in a 10-m-wide drainage channel immediately to the northwest of the offset ridge (Fig. 4). We centered our attention on the northeast strand of the fault because it accommodated the majority of late-Quaternary offset and the coseismic offset in 1956. The location of each trench in relation to the fault trace is shown in detail in Figure 7. Within the trenches, the displacement is accommodated by several, subparallel fractures that are expressed at the surface by a low (20 cm) scarp along a 2-m-wide linear pressure ridge. The faults observed within the trenches were well defined by the truncation or displacement of stratigraphic contacts (Figs. 8a and 8b). Examination of the fault-parallel trenches provided the basis to define the sense of slip and offset in the 1956 sequence and to place age constraints on the time of the penultimate event.

Slip from the 1956 Surface Rupture

Trench T-3 parallels the fault on the upstream and upthrown northeastern block (Fig. 7). The active channel (Qya_1, not shown in Fig. 7 for simplicity) is continuous and undeformed across the fault at this location. Deposits of the active channel are not broken but thicken abruptly on the downthrown side of the fault and overlay a sequence of buried channel fill deposits (Qya_2, Qya_3) (Fig. 9). Two charcoal samples were collected from stratified alluvium below Qya2 that yielded dendrochronologically corrected radiocarbon ages of $675^{+105}/_{-212}$ yr B.P. (sample ^{14}C-7) and $590^{+111}/_{-76}$ yr B.P. (sample ^{14}C-17) (Fig. 9). All charcoal samples in this study were calibrated using CALIB 3.0 by Stuiver and Reimer (1993) with 2σ error range. The nested character of channel deposits Qya_2 and the underlying alluvium suggests that they were deposited within a short interval of time. We further interpret that the source of the buried Qya_2 channel is the same as the present-day active

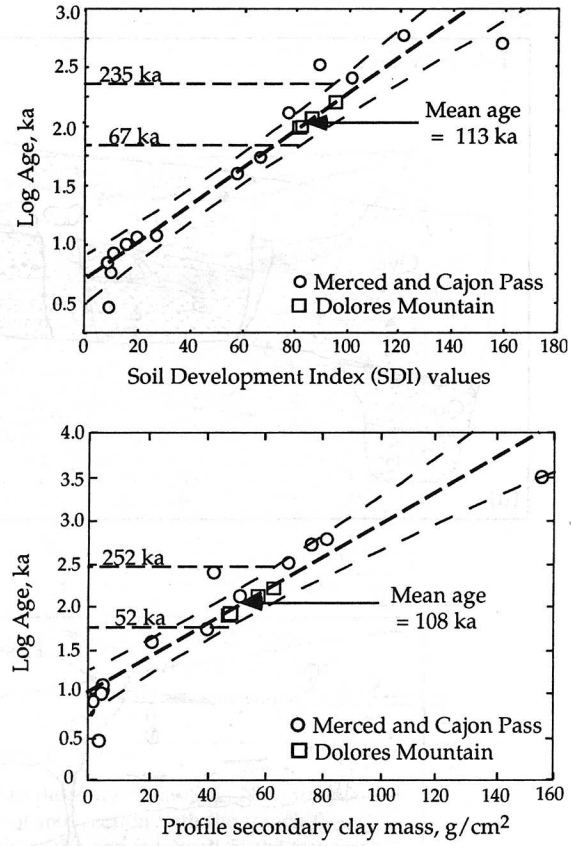

Figure 6. Comparison of soils at Merced and Cajon Pass (open circles) to determine log age of Dolores Mountain profiles (open squares). Dashed lines are 95% (2σ) error bounds on the least-squares regressions.

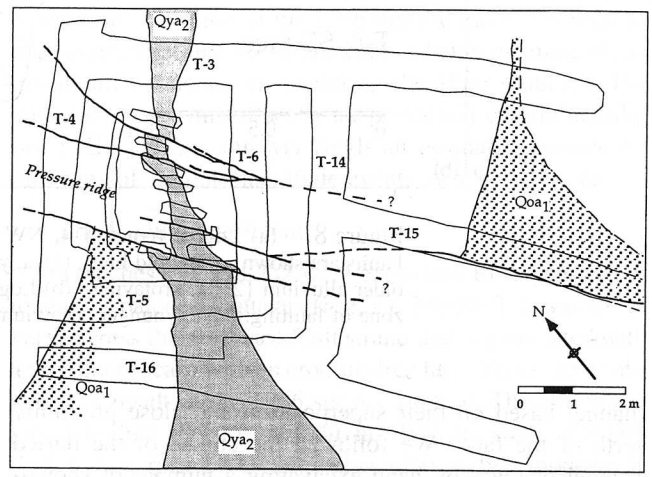

Figure 7. Trenches and offset channels Qya2 and Qoa1. Only the NW margin of Qoa1 is displayed on the southwest side of the fault for simplicity. The feeder channel for Qoa1 is narrow upstream to the NE and widens as it passes through the fault zone to the SW. Fissuring from the penultimate event in T-5 and Qya1 are not shown for simplicity. Small, unlabeled trenches are T-7 through T-13.

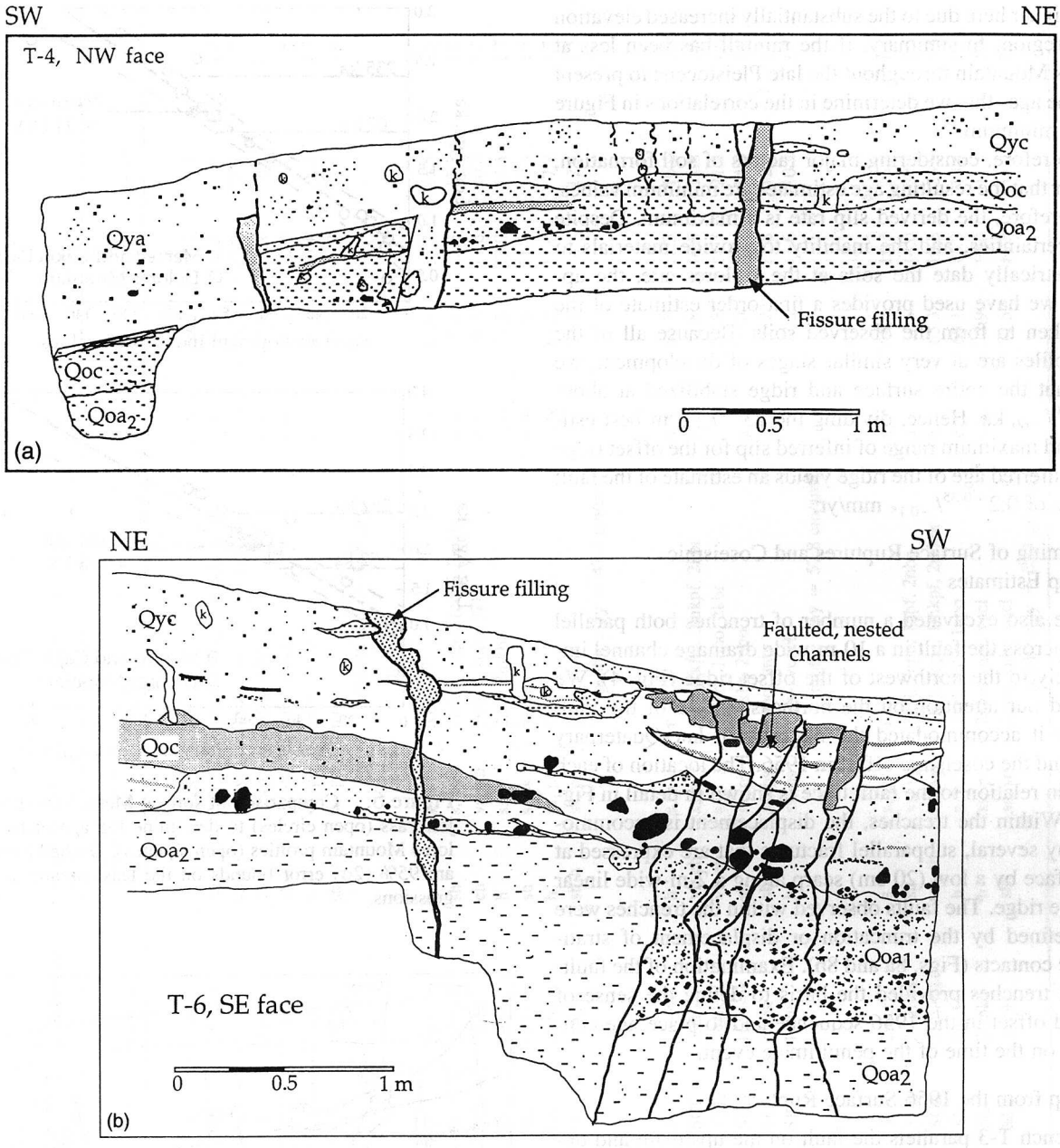

Figure 8. (a) Log of trench T-4, NW face perpendicular to the zone of faulting. Faults are shown using bold lines. (Qya, young alluvium; Qoc, older colluvium; Qoa_2, older alluvium {2}; *k*, krotavina). (b) Log of trench T-6, SE face perpendicular to the zone of faulting. (Qyc, younger colluvium; Qoa1, older alluvium {1}).

channel based on their superposition and close proximity north of the fault. We followed the course of the buried channel of Qya_2 by hand excavating a number of shovel-width trenches across the fault zone (Fig. 7). An electronic survey of the margins of this buried channel deposit shows that it is offset right laterally. A best estimate of the slip is determined by reconstruction of the offset northwest margin of the channel that yields about 115 cm of dextral slip (Fig. 10). Offset of the southeast margin appears to be less, about 80 cm, but is a little problematic because the channel margin trends nearly parallel to the southern fracture where it is displaced. Errors in measuring the offsets are negligible due to the density of surveying points used to document the location of the Qya2 channel margin.

Total vertical displacement across the entire zone of faulting, when accounting for the gradient of the channel, is less than 10 cm. We interpret that the 80 to 115 cm of right-lateral slip represents displacement during the 1956 earthquake sequence, which is slightly larger than that reported by Shor and Roberts (1958); they originally measured a

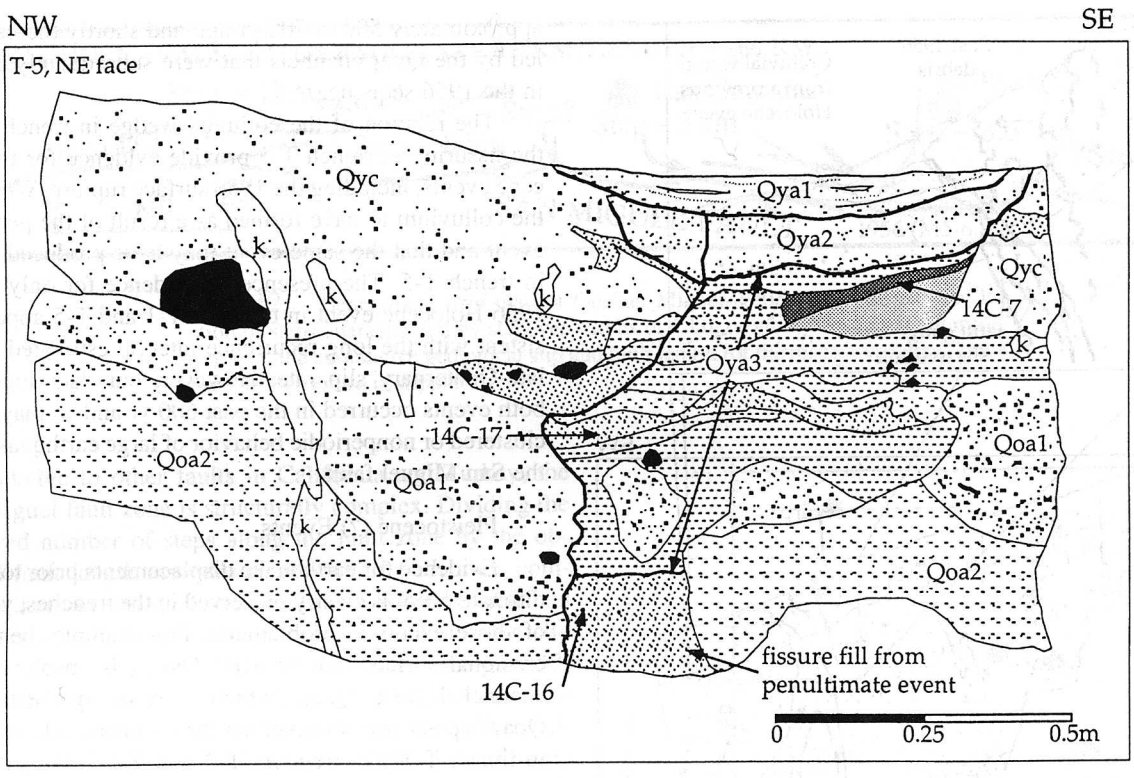

Figure 9. Log of trench T-5, NE face parallel to the zone of faulting. Note irregularity of minor fault trace is due to its low angle of intersection with the trench face. Sample 14C-17 was recovered from the same unit on the opposite wall of the trench. Faults are shown using bold lines. (Qya1, young alluvium {1}; Qya2, young alluvium {2}; Qya3, young alluvium {3}).

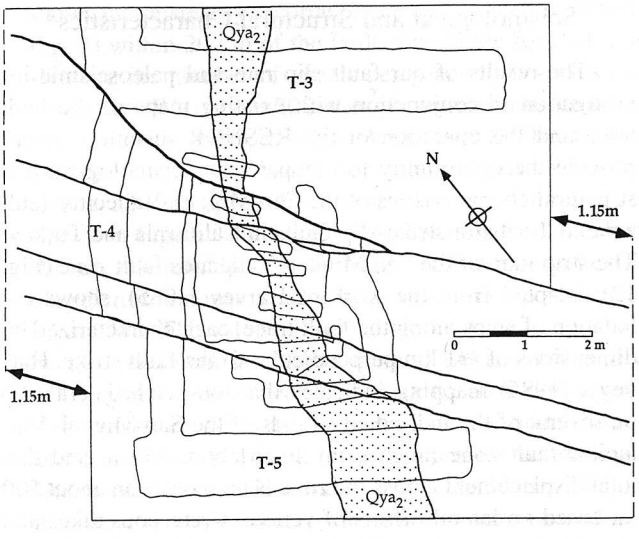

Figure 10. Trench site with the reconstruction of the northwest margin of the channel. Trenches excavated later in the study (as in Fig. 7) are omitted from the drawing.

maximum strike-slip offset of 79 cm but provided no observations at Dolores Mountain, perhaps because of the lack of clear offset features. Because Dolores Mountain is located in the central portion of the 1956 rupture trace, it is reasonable to interpret that 80 to 115 cm is a better estimate of the maximum coseismic offset during the 1956 sequence. Dividing the coseismic offset by the previously determined slip rate ($0.2^{+0.35}/_{-0.15}$ mm/yr) yields an estimated average return time of similar magnitude events of $5.8^{+17}/_{-4.3}$ ka.

The Penultimate Event

Trenches T-1 and T-2 were excavated to search for evidence of paleoearthquakes (Fig. 4). Trench T-1 was excavated across the northeast fault strand that is associated with a prominent scarp with an eroding-free face. This scarp probably is a result of the 1956 surface rupture. The trench exposed faulted Pleistocene alluvial deposits and colluvium (Fig. 11) overprinted by a soil characterized by a moderately well-expressed, reddened, clay-rich B_t horizon. The strength of the soil development is interpreted to indicate a pre-Holocene age for the majority of units exposed in the trench. In trench T-1, there is a wedge-shaped deposit of colluvium and *A* soil horizon material that is faulted by the southern fracture that displays reverse separation (Fig. 11). Because this deposit is faulted, it must have been present prior to the

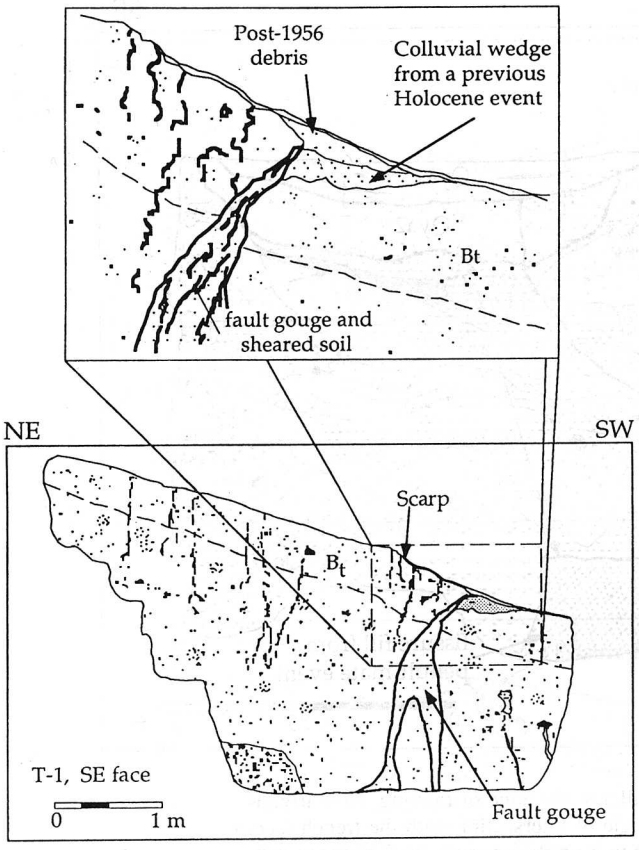

Figure 11. Log of trench T-1, SE face perpendicular to the fault scarp and a close up of the colluvial wedge and soil units. The faulting from the 1956 surface rupture goes up to the surface and has faulted the preexisting colluvial wedge, thereby demonstrating the existence of at least one prior, probably Holocene event.

1956 earthquake, thereby indicating the presence of a penultimate, probable Holocene event. This colluvium immediately overlies the reddened clay-rich B_t horizon, and is, therefore, the only Holocene deposit exposed in trench T-1. The well-developed, clay-rich B_t horizon, which took many thousands of years to form, is undisturbed by rupturing prior to the penultimate event.

Evidence for a penultimate event is also preserved in the trenches excavated in the modern channel (Fig. 9). The event is indicated by the presence of a number of infilled fractures that underlie the channel sequence (Qya_2 and Qya_3) that was offset in the 1956 earthquake. The presence of horizontal stratification in the infill of one of the fissures is the basis to interpret that the fissures were subject to surface flow of water after fissuring. The calibrated age of charcoal collected from within the stratified fissure fill is $610^{+59}/_{-99}$ yr B.P. (sample ^{14}C-16) (Fig. 9). The calibrated ages of charcoal samples recovered from the overlying channels are $675^{+105}/_{-212}$ yr B.P. (sample ^{14}C-7) and $590^{+111}/_{-76}$ yr B.P. (sample ^{14}C-17), indistinguishable from sample ^{14}C-16 (Fig. 9). We thus interpret that the fissures were produced approximately 500 to 700 yr ago and shortly thereafter buried by the Qya_2 channels that were subsequently displaced in the 1956 sequence.

The relation of the colluvial wedge in trench T-1 and the fissuring in trench T-5 provide evidence for two Holocene events, including the 1956 surface rupture. We interpret the colluvium to have formed as a result of the penultimate event and that the same event may have produced fissuring in trench T-5. The presence of evidence for only one pre-1956 Holocene event in trenches T-1 and T-5 appears consistent with the long recurrence interval estimated from the late-Quaternary slip rate. However, our data suggest that both events occurred in the past 600 yr and so may reflect a clustered or nonperiodic behavior of large earthquakes along the San Miguel fault.

Pleistocene (?) Events

Evidence for earthquake displacements prior to the penultimate event is clearly preserved in the trenches, yet dating of those events is problematic. For example, beneath the erosional surface that predates Qya_{1-3} is an older, faulted channel deposit (Qoa_1), which is offset by the fault. The Qoa_1 deposit was observed on the northeast side of the fault in trench T-15, in trenches T-4 and T-6, and in the lower portions of trenches T-5 and T-16 (Figs. 7 through 9). The unit is distinguished in the field by its coarse gravelly sand texture and a distinct reddish iron staining. The Qoa_1 channel is offset 7.5 m in a right-lateral sense and 30 cm vertically, yielding a lateral-to-vertical slip ratio of 25:1, similar to the ratio observed for the offset alluvial ridgeline (40:1). We were unable to determine the age of the channel nor exactly how many events produced the 7.5 m of displacement. Nevertheless, these observations demonstrate that the long-term sense of slip is predominantly dextral.

Seismological and Structural Characteristics

The results of our fault slip rate and paleoseismic investigation in conjunction with existing maps of the fault trace and the operation of the RESNOR seismic network provide the opportunity to compare the seismological and structural characteristics of the San Miguel–Vallecitos fault zone to the major strike-slip faults in California and Turkey. The strip map of the San Miguel–Vallecitos fault zone (Fig. 12), adapted from the work of Harvey (1985), shows the location of steps along the fault trace, each characterized by dimensions of $\geq$1 km perpendicular to the fault strike. Harvey's (1985) mapping indicates that total right-lateral slip on several of the individual strands of the San Miguel–Vallecitos fault zone range from 20 to about 250 m and that total displacement across the zone is no more than about 500 m, based on lateral offsets of vertical Cretaceous dikes and vertical displacement of Miocene and older volcanic surfaces and deposits. Recent studies (Giroux, 1993; Hirabayashi *et al.*, 1993) yield similar results with a total slip of about 575 m determined from offset of basement rock.

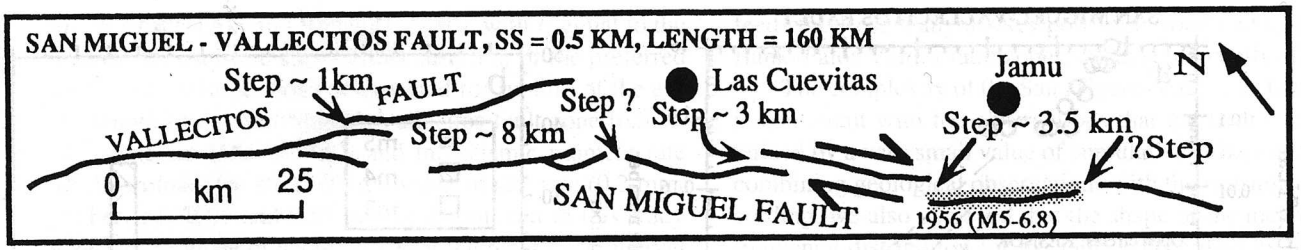

Figure 12. Generalized strip map of the San Miguel–Vallecitos fault marking location of steps characterized by stepover widths of 1 km or greater and showing information on the cumulative geological slip and fault length for the respective faults. Trace of the 1956 rupture is stippled.

Relative to other faults in California and Turkey, the San Miguel fault zone is structurally complex. Dividing the observed number of steps along the fault zone by the observed fault length provides a measure of fault trace complexity that can be directly compared to previously published estimates of fault-trace complexity for the major strike-slip faults of California (e.g., Wesnousky, 1988). In Figure 13, we plot the number of steps per kilometer versus cumulative geologic offset along the San Miguel–Vallecitos fault to values previously reported for strike-slip faults in California and Turkey. The greater complexity of the San Miguel–Vallecitos fault in relation to faults in California and Turkey is consistent with the idea that fault-trace complexity decreases with greater geologic offset.

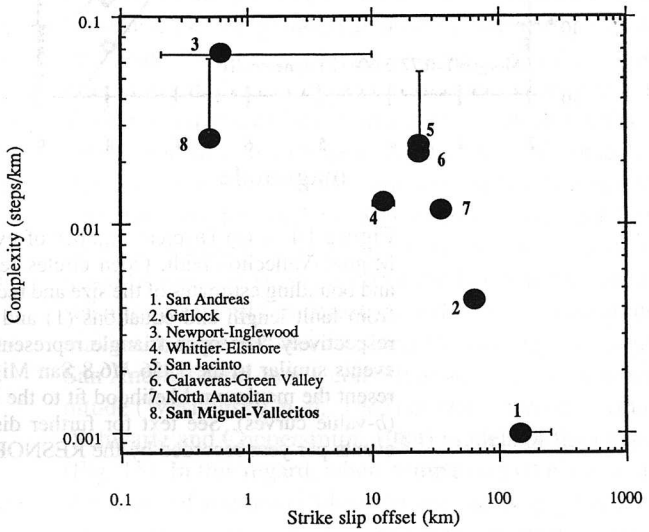

Figure 13. Fault-trace complexity measured as the number of steps ≥1-km width (closed symbols) per unit length of fault trace is plotted versus cumulative geologic offset for the San Miguel–Vallecitos fault and major strike-slip faults in California and Turkey. Error bars represent uncertainties in the number of steps along the fault traces and in the amount of cumulative slip.

Effective instrumental monitoring of seismicity in the vicinity of the San Miguel–Vallecitos fault began in 1976, with the development of the digitally recorded, three-component RESNOR (Red Sismica Del Noroeste De Mexico) seismic network in northwestern Mexico (Fig. 1). The epicentral distribution of events recorded by RESNOR during the period 1976 to 1991 is plotted in Figure 2. Figure 14a shows the seismicity recorded (i.e., within the box shown in Fig. 2) within 20 km of the fault zone in the form of a plot showing the number of events per year (n/yr) versus magnitude (M). We choose 20 km as our search limits, consistent with the methodology used by Wesnousky (1994), to define the seismicity rates of faults in southern California. For reference, a histogram of the number of events per year also is shown in Figure 14b. Lines of the form of the Gutenberg–Richter relationship Log n/yr $= a - bM$ are fit and extrapolated from the instrumental data shown by open circles in Figure 14a. The value of b is the slope of the line and is fit by the maximum likelihood method (Aki, 1965) and the value a (productivity) is fit to satisfy the total number of $M > 3$ events reported during the recording period. The solid and dashed lines in Figure 14a thus represent the maximum-likelihood fit to the data and the 95% confidence limits for that fit. For convenience, the line fits are referred to as "b-value curves" in the remainder of the report. The total number (N) of events used to determine the b-value, the estimated b-value and 95% confidence limits, and the instrumental seismic moment release rate $\dot{M}_o$ (*instr*) over the period of instrumental recording are listed in the lower left of each of the plots. The instrumental seismic moment release rate is the sum of the seismic moments of all recorded events of magnitude greater than or equal to 3 divided by the number of years of recording, where the seismic moment of each event is determined from its magnitude by use of the relationship Log $M_o = 1.5M + 16.1$ (Hanks and Kanamori, 1979).

The period that the RESNOR network has been recording is much less than the expected return time of M6.8 and greater earthquakes. Toward estimating the recurrence time of such events, it is common practice to extrapolate to larger magnitudes with b-value curves that have been calculated on the observation of more frequently occurring but lesser-sized events. It is useful to compare the predictions of the b-value curves for the San Miguel–Vallecitos fault zone

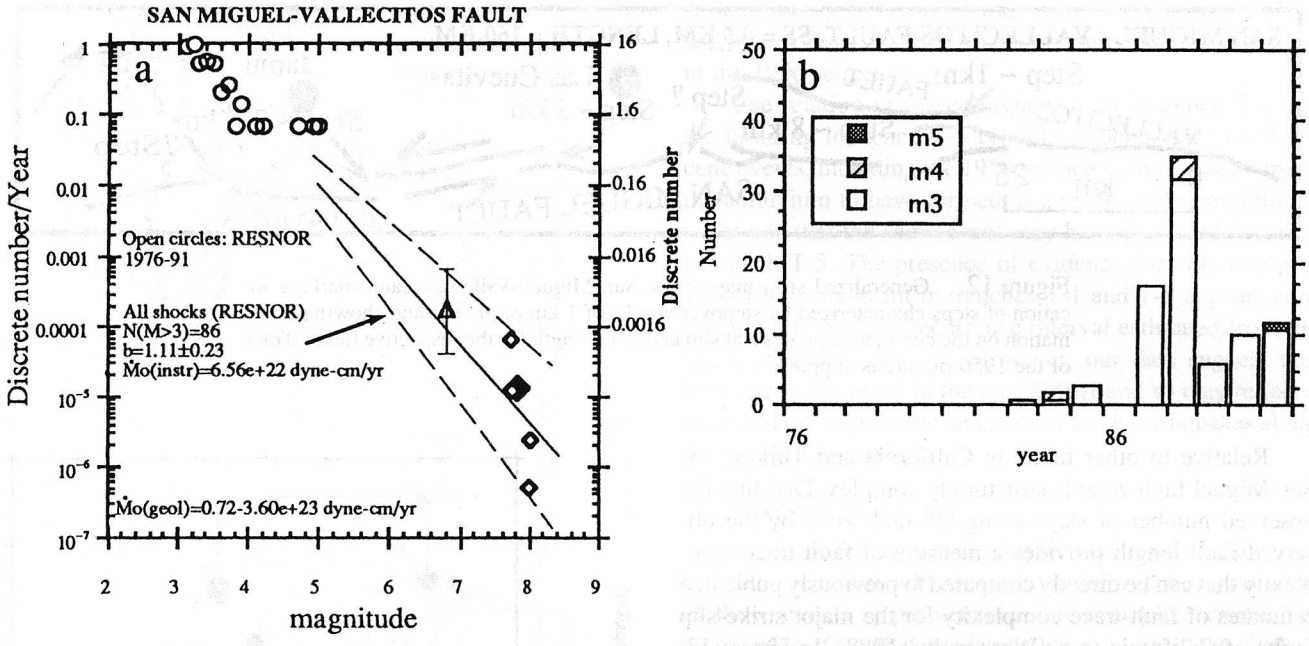

Figure 14. (a) Discrete number of events per year versus magnitude for the San Miguel–Vallecitos fault. Open circles represent the instrumental data. The preferred and bounding estimates of the size and recurrence rate of maximum earthquakes derived from fault length and equations (1) and (2) are shown as solid and open diamonds, respectively. The open triangle represents the size and recurrence rate estimated for events similar to the 1956 M6.8 San Miguel earthquake. Solid and dashed lines represent the maximum-likelihood fit to the instrumental data, and 95% confidence limits (b-value curves). See text for further discussion. (b) Histogram showing number of events per year recorded by the RESNOR network.

(Fig. 14) to the constraints we may impose on the recurrence characteristics of the largest expected earthquakes from our geological observations. From the prior geological observations, we estimate an approximate recurrence interval of 1956-type M6.8 earthquakes of $5.8\ ^{+17}/_{-4.3}$ ka. The size and recurrence rate is indicated by the open triangle in Figure 14a. The open triangle also falls within the 95% confidence limits of the b-value curves determined from the instrumental data set. This latter observation is consistent with the interpretation that the seismicity along the San Miguel–Vallecitos fault satisfies a Gutenberg–Richter relationship Log $n = a - bM$ for magnitudes between about 3 and 6.8.

A similar approach may be taken with the assumption that the maximum expected event ruptures the entire 160-km length of the San Miguel–Vallecitos fault zone. The seismic moment of such an event (M_o^e) is estimated by use of a recently developed equation of moment magnitude versus fault length and slip rate (Anderson *et al.,* 1996), the seismic moment again converted from moment magnitude by use of the relationship log $M_o = 1.5Mw + 16.1$ (Hanks and Kanamori, 1979). Bounds on the expected seismic moment M_o^e for such an event may be placed at between 4.5×10^{27} dyne-cm ($Mw = 7.7$) and 1.3×10^{28} dyne-cm ($Mw = 8.0$), with a most likely or preferred value equal to 6.3×10^{27} dyne-cm ($Mw = 7.8$). The upper bound is unlikely because of the amount of coseismic slip that would be required to produce an event of that magnitude on the 160-km-long fault.

The recurrence interval T of such events along the fault zone may be estimated by dividing the cumulative seismic moment release ΣM_o expected during the recurrence interval T by a geologically determined average seismic moment rate $\dot{M}_o^g$ for the fault

$$T = \Sigma M_o / \dot{M}_o^g = (M_o^e)/\dot{M}_o^g, \quad (1)$$

which may also be written as

$$T = (M_o^e/\dot{M}_o^g)/[1 - (\dot{M}_o^{sm}/\dot{M}_o^g)], \quad (2)$$

where M_o^e is the seismic moment of the maximum expected event, ΣM_o^{sm} is the sum of the seismic moment release of events with $M_o < M_o^e$, which will contribute to fault slip during the recurrence interval T, and $\dot{M}_o^{sm}$ is approximated by the empirically determined instrumental moment release rate $\dot{M}_o$ (*instr*). The seismic moment rate $\dot{M}_o^g$ is estimated by the relationship $\dot{M}_o^g = \mu LW\,\dot{U}^g$, whereby μ is the shear modulus (assumed to equal 3×10^{11} dyne/cm^2), L is the fault length, W is the fault width (approximated to 15 km), and $\dot{U}^g$ is the geologically determined slip rate (e.g., Brune, 1968). The equation is a modified version of the relationship

$M_0 = \mu LWU$ (Aki and Richards, 1980), with U equal to the amount of coseismic slip. Further insertion of the preferred estimate of seismic moment expected for rupture of the entire length of the San Miguel–Vallecitos fault zone [6.3×10^{27} dyne-cm ($Mw = 7.8$)] and the seismic moment rate $\dot{M}_o^g$ determined for the preferred value of slip rate (0.2 mm/yr) between 0.05 and 0.55 mm/yr determined in this study yields an estimate of about 80 ka for the recurrence interval between such events. The estimate of recurrence interval and expected moment magnitude ($Mw = 7.8$) are represented by the solid diamond in Figure 14a. Bounds on the estimate are represented by the four open diamonds in Figure 14a and reflect the insertion of the minimum and maximum bounds on both the expected seismic moment and geologically assessed seismic moment rate into equation (2). The bounds on earthquake size and recurrence rate represented by the open and closed diamonds fall within the 95% confidence limits of the b-value lines extrapolated from the instrumental record of seismicity. Hence, if we assume that (1) the rate of small to moderate earthquakes is reflected in the recording period of the RESNOR network and (2) our calculations based on the fault length and fault slip rate correctly approximate the size and return time of the largest possible events along the San Miguel–Vallecitos fault zone, the seismicity along the San Miguel–Vallecitos fault zone is satisfactorily described by the Gutenberg–Richter relationship.

Discussion and Conclusions

The principal results of the fieldwork are that the slip rate for the San Miguel–Vallecitos fault is quite low relative to other strike-slip faults in northern Baja California and southern California (Petersen and Wesnousky, 1994), and the consequent return time for large earthquakes is long. For instance, the slip rate for the Agua Blanca fault has been estimated at about 6 mm/yr, using similar criteria as those applied in this study (Rockwell *et al.*, 1987, 1993). Thus, the San Miguel–Vallecitos fault appears to transfer less than 1% of the plate motion and contributes only minor slip to the Inner Continental Borderland system of faults offshore from southern California.

The slip rate on the Rose Canyon fault has been determined at about 1.5 mm/yr based on trenching in early-Holocene deposits in San Diego (Rockwell *et al.*, 1990; Lindvall and Rockwell, 1995). This rate is at least several times the rate that we determined for the San Miguel–Vallecitos fault. Thus, the notion that the San Miguel–Vallecitos fault zone is the southern continuation of the Rose Canyon fault is oversimplified. The San Miguel–Vallecitos is not directly continuous with the Rose Canyon fault zone in San Diego, and most of the Rose Canyon slip probably transfers from the offshore faults that are fed by slip on the Agua Blanca fault zone. Even when the San Miguel–Vallecitos slip rate is combined with that of the Agua Blanca fault, the rate estimated by Rockwell *et al.* (1993) for the inner Continental Borderland system of faults, part of which directly feeds the Rose Canyon–Newport Inglewood and Coronado Bank–Palos Verdes fault zones, is not significantly affected.

The complexity of the San Miguel–Vallecitos fault trace is consistent with the observations that the fault is characterized by a very small value of cumulative strike slip. When combining geological observations with the instrumental recording, we also observed that the shape of the magnitude–frequency distribution for the fault is described by the Gutenberg–Richter relationship. The same approach was used earlier to define the magnitude–frequency distribution of faults in southern California (Wesnousky, 1990, 1994). In contrast, it was generally observed for major southern California faults that the preferred estimates of the frequency of occurrence of the largest expected earthquakes resulting from analysis of geological observations along the major strike-slip faults of southern California generally fall above maximum-likelihood estimates of the recurrence rate of similar-sized events based on extrapolation of b-value lines determined from lesser-sized events. The difference is manifest most strongly when comparing the San Miguel–Vallecitos fault to the southern San Andreas fault and Garlock faults of southern California, where extrapolation of earthquake frequency statistics from the instrumental record of seismicity severely underestimate the rate of occurrence of maximum expected events along the Garlock and southern San Andreas fault zones, consistent with the maximum magnitude (Wesnousky *et al.*, 1983) or characteristic earthquake (Schwartz and Coppersmith, 1984) models of fault behavior (Fig. 15). In this regard, when compared to the major strike-slip faults of southern California, the San Miguel–Vallecitos fault zone appears to be enriched in the occurrence of small- to moderate-sized events relative to the occurrence of the largest expected events along the fault. Specifically, when comparing the annual productivity of $M3$ events (normalized with respect to fault length and slip rate, i.e., n/yr/length/rate) along the San Miguel–Vallecitos, southern San Andreas and Garlock faults, we observe that the productivity of the San Miguel–Vallecitos fault (0.0354) is 50 to 70 times greater than the other faults (San Andreas fault = 0.0007, Garlock fault = 0.0005). It is possible that the enrichment of small to moderate events is not characteristic of seismicity along the San Miguel–Vallecitos fault over the entire return period of maximum-sized events of the fault but, rather, reflects simply an insufficient instrumental record of recording. In this respect, it may also be hypothesized that we are observing an extended aftershock sequence following the 1956 earthquake. However, when noting that cumulative strike-slip fault offset along the Garlock and San Andreas fault is measured in many tens of kilometers as compared to 0.5 km for the San Miguel–Vallecitos fault, it seems reasonable to speculate that the increased productivity of small earthquakes along the San Miguel–Vallecitos fault reflects a more heterogeneous stress field associated with the incipient nature of the fault, or perhaps that extended aftershock sequences characterize faults with small amounts of cumulative slip.

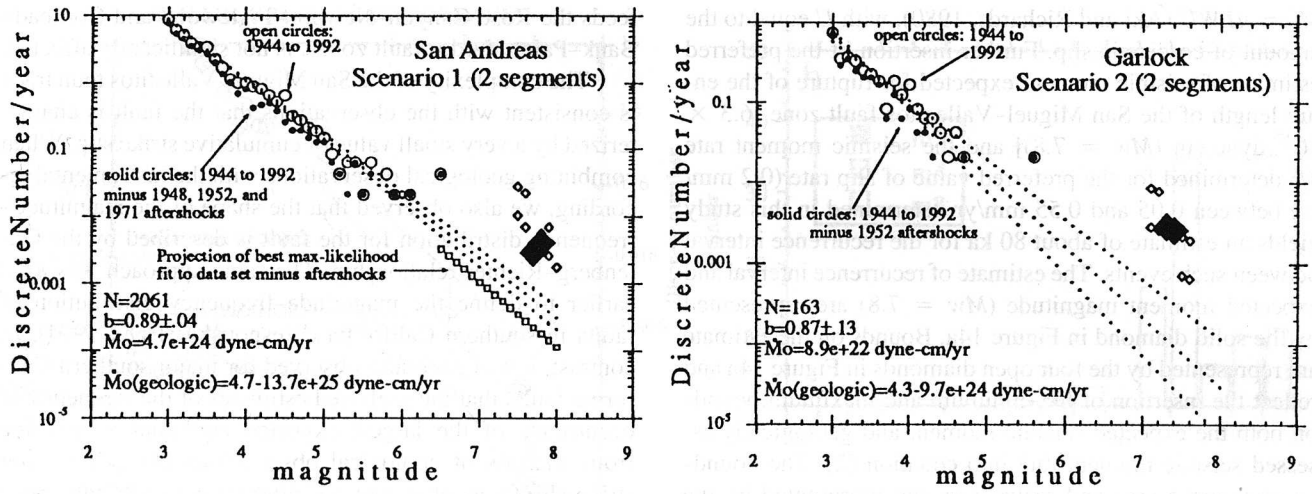

Figure 15. Discrete number of events per year versus magnitude for the Garlock and San Andreas faults of southern California (taken from Wesnousky, 1994). Seismicity within approximately 20-km-wide boxes along the faults, similar to that used for San Miguel in Figure 14, were used to construct the figure. See Figure 14 for explanation.

Acknowledgments

We thank Jim Brune, John Anderson, and Gordon Gastil for discussions during the early stages of this work. Kevin Bryan, along with the 1993 SDSU neotectonics class, excavated voluminous quantities of soil to provide trench exposures. Comments on the manuscript by Russell Wheeler, Keith Kelson, and James Dolan improved the manuscript significantly. Raul Castro (CICESE) provided us with the RESNOR instrumental seismicity data. Center for Neotectonic Studies Contribution No. 16. The research was supported by USGS Contracts 1434-92-G-2222 and 1434-92-G-2223.

References

Aki, K. (1965). Maximum likelihood estimates of b in the formula logN = a − bM and its confidence limits, *Bull. Earthquake Res. Inst.* **43,** 237–239.

Aki, K. and P. G. Richards (1980). *Quantitative Seismology: Theory and Methods,* W.H. Freeman, San Francisco, 1–932.

Anderson, J. G., S. G. Wesnousky, and M. W. Stirling (1996). Earthquake size as a function of fault slip rate, *Bull. Seism. Soc. Am.* **86,** 000–000.

Birkeland, P. W. (1984). *Soils and Geomorphology,* Oxford University Press, New York, 372 pp.

Brune, J. N. (1968). Seismic moment, seismicity and rate of slip along major fault zones, *J. Geophys. Res.* **73** (2), 777–784.

Doiser, D. I. (1992). Faulting processes of the 1956 San Miguel, Baja California, earthquake sequence, *Pageoph* **139** (1), 3–16.

Gastil, R. G., R. P. Phillips, and E. C. Allison (1975). Reconnaissance geology of the state of Baja California, *Geol. Soc. Am. Memoir 140.*

Giroux, B. K. (1993). Net slip on the San Miguel fault near Los Ojos Negros, northern Baja California: implications for initiation age of faulting, *B.S. Thesis,* San Diego State University, unpublished.

Hanks, T. C and H. Kanamori (1979). A moment magnitude scale, *J. Geophys. Res.* **84,** 2348–2350.

Harden, J. W. (1982). A quantitative index of soil development from field descriptions: examples from a chronosequence in central California, *Geoderma* **28,** 1–28.

Harrison, J. B., L. D. McFadden, and R. J. Weldon III (1990). Spatial soil variability in the Cajon Pass chronosequence: implications for the use of soils as a geochronological tool, *Geomorphology* **3,** 399–416.

Harrison, J. B., L. D. McFadden, and R. J. Weldon III (1993). The influence of colluvial deposition on rates of soil development in the Transverse Ranges, southern California, *Isr. J. Earth Sci.* **41,** 139–154.

Harvey, T. W. (1985). Geology of the San Miguel fault zone, northern Baja California, Mexico: *Master's Thesis,* San Diego State University, p. 330, unpublished.

Hirabayashi, C. K. (1995). Quaternary activity of the San Miguel fault, northern Baja California, Mexico, *Master's Thesis,* San Diego State University, 81 pp, unpublished.

Hirabayashi, C. K., B. K. Giroux, and T. K. Rockwell (1994). Total slip across the San Miguel fault, northern Baja California: implications for the initial age of faulting (abstracts with programs), *Geol. Soc. Am.* **26** (2), 59.

Hirabayashi, C. K., T. K. Rockwell, and S. Wesnousky (1993). Clustering of seismic activity on the San Miguel fault, Baja California, Mexico, *EOS AGU Fall Supplement,* 575.

Johnson, D. L. and D. Watson-Stegner (1987). Evolution model of pedogenesis, *Soil Sci.* **143,** 349–366.

Johnson, D. L., E. A. Keller, and T. K. Rockwell (1990). Dynamic pedogenesis: new views on some key soil concepts, and a model for interpreting Quaternary soils, *Quat. Res.* **33,** 306–319.

Johnson, T. L., J. Madrid, and T. Koczynski (1976). A study of microseismicity in northern Baja California, Mexico, *Bull. Seism. Soc. Am.* **66,** 1921–1929.

Lindvall, S. C and T. K. Rockwell (1995). Holocene activity of the Rose Canyon fault, San Diego, California, *J. Geophys Res.* **100** (12), 24121–24132.

McFadden, L. D. and R. Weldon (1987). Rates and processes of soil development on Quaternary terraces in Cajon Pass, California, *Geol. Soc. Am. Bull.* **98,** 280–293.

Minch, J. A. (1979). The late Mesozoic–early Tertiary framework of continental sedimentation, northern Peninsular Ranges, Baja California, Mexico, in *Earthquakes and Other Perils, San Diego Region, San Diego Association of Geologists Guidebook for the 1979 National GSA Meeting,* P. L. Abbott (Editor), Fidelity Printing, San Diego, 43–67.

Peterson, M. D. and S. G. Wesnousky (1994). Fault slip rates and earthquake histories for active faults in southern California, *Bull. Seism. Soc. Am.* **84,** 1608–1649.

Reheis, M. C., J. W. Harden, L. D. McFadden, and R. Shroba (1989). De-

velopment rates of late Quaternary soils, Silver Lake Playa, California, *Soil Sci. Soc. Am. J.* **53,** 1127–1140.

Reyes, A., J. N. Bruen, T. Barker, L. Canales, J. Madrid, J. Revollar, and L. Munguia (1975). A microearthquake survey of the San Miguel fault zone, Baja California, Mexico, *Geophys. Res. Lett.* **2** (2), 56–59.

Rockwell, T. K., D. L. Johnson, E. A. Keller, and G. R. Dembroff (1985). A late Pleistocene-Holocene soil chronosequence in the central Ventura Basin, southern California, U.S.A., in *Geomorphology and Soils,* K. Richards, R. Arnett, and S. Ellis (Editors), George Allen and Unwin, 309–327.

Rockwell, T. K., M. E. Hatch, and D. L. Schug (1987). Late Quaternary rates: Agua Blanca and borderland faults, U.S. Geological Survey Final Technical Report for Contract No. 14-08-0001-22012, 122 pp.

Rockwell, T. K. and Scott Lindvall (1990). Holocene activity of the Rose Canyon fault in San Diego, California, based on trench exposures and tectonic geomorphology (abstracts with programs), *Geol. Soc. Am.* **22,** (3), 78.

Rockwell, T. K., C. Loughman, and P. Merifield (1990). Late Quaternary rate of slip along the San Jacinto fault zone near Anza, southern California, *J. Geophys. Res.,* **95,** 8593–8605.

Rockwell, T. K., D. L. Schug, and M. E. Hatch (1993). Late Quaternary slip rates along the Agua Blanca fault, Baja California, Mexico, in *Geological Investigations of Baja California,* P. L. Abott (Editor), South Coast Geological Society, Annual Field Trip Guidebook No. 21, 53–92.

Schwartz, D. P. and K. J. Coppersmith (1984). Fault behavior and characteristic earthquakes: examples from the Wasatch and San Andreas fault zones, *J. Geophys. Res.* **89,** 5681–5698.

Shor, G. G. and E. Roberts (1958). San Miguel, Baja California Norte earthquakes of February 1956, A field report, *Bull. Seism. Soc. Am.* **48,** 101–116.

Soil Survey Staff (1975). *Soil Taxonomy, U.S. Department of Agriculture Handbook 436,* U.S. Government Printing Office, Washington, D.C., 754 pp.

Vidal, A. and L. Munguia (1991). Local magnitude and source parameters for earthquakes in the Peninsular Ranges of Baja California, Mexico, *Bull. Seism. Soc. Am.* **81,** 2254–2267.

Wesnousky, S. G. (1988). Seismological and structural evolution of strike-slip faults, *Nature* **355,** 340–343.

Wesnousky, S. G. (1990). Seismicity as a function of cumulative geologic offset: some observations from southern California, *Bull. Seism. Soc. Am.* **80,** 1374–1381.

Wesnousky, S. G. (1994). The Gutenburg–Richter or characteristic earthquake distribution, which is it?, *Bull. Seism. Soc. Am.* **84** (6), 1940–1959.

Wesnousky, S. G., C. H. Scholz, K. Shimazaki, and T. Matsuda (1983). Earthquake frequency distributions and the mechanics of faulting, *J. Geophys. Res.* **88** (B11), 9331–9340.

Department of Geological Sciences
San Diego State University
San Diego, California 92182
(C. K. H., T. K. R.)

Center for Neotectonic Studies
Department of Geological Sciences
University of Nevada, Reno
Reno, Nevada 89557
(S. G. W., M. W. S.)

Department of Geology, Earth Sciences Division,
CICESE, Km. 107, Carretera Tijuana-Ensenada,
Ensenada, Baja California, Mexico
(F. S.-V.)

Manuscript received 10 April 1995.